An Optical Disdrometer for the Measurement of Raindrop Size Spectra in Windy Conditions

A. J. ILLINGWORTH AND C. J. STEVENS

Department of Physics UMIST, Manchester M60 1QD, England

(Manuscript received 13 May 1986, in final form 8 January 1987)

ABSTRACT

An instrument for measuring the size and concentration of raindrops is described which has the ability to function equally well in calm conditions and strong winds. Raindrops are detected optically in a shadowgraph-type imaging system. A unique feature of the device is the sensing of drop size as drops enter and leave a cylindrical sample volume. Each drop produces two equally sized pulses, the heights of which are proportional to the drop's diameter and their separation yields the drop's transit time. The drop concentration can be derived from this data without assuming or measuring drop velocities. The instrument has a large sample volume, but a negligible loss of data resulting from two drops being sampled simultaneously. Drops above 300 μm can be detected, but beam divergence limits accurate sizing to drops larger than 400 μm. Laboratory calibration shows that drops greater than 1 mm in diameter may be sized to better than 5%. Comparison tests with a tipping bucket raingage reveal that time integrations of the raindrop size spectra yield rainfall totals generally within 10% of the bulk-measured values. These tests also show that disdrometers which sense raindrop flux will seriously overestimate drop concentrations in windy conditions but that this new device performs satisfactorily for winds of up to 20 m s^{-1}.

1. Introduction

Measurements of the raindrop size distribution are of value in the interpretation of radar signals, in predicting the attenuation of electromagnetic radiation, and because of the information such data provide on the mechanisms responsible for the production and modification of naturally occurring rainfall. It is important that such observations can be made reliably in both calm and windy conditions. For over 90 years, since Lowe (1902), instruments have been constructed which are capable of measuring raindrop sizes and number concentrations both at the ground and above. All such instruments rely on the measurement of the flux of differently sized drops, and the conversion to a drop concentration is made using measured or assumed drop velocities. In section 2 of the paper, we review the performance of such instruments in winds of up to 20 m s^{-1}. The principle of operation of an instrument which should function more satisfactorily in high windspeeds is outlined in section 3, and the physical details of such a device are described in section 4. In section 5, we consider the statistical and signal processing requirements of the instrument and how these may be implemented. Section 6 analyzes the effect of beam divergence and diffraction on its operation. The calibration of the instrument is described in section 7, and some results of field testing which validate its performance are provided in section 8.

2. Review of existing disdrometers

Two devices that summarize the principles upon which most raindrop disdrometers operate are the electromechanical impaction type designed by Joss and Waldvogel (1967) (J–W), and the Knollenberg Optical Array spectrometer (Knollenberg, 1970), which uses the shadowgraph imaging technique. There are several conflicting requirements that must be reconciled for optimum response. The raindrop size distribution generally falls off exponentially with size, and so a large sample area is needed to obtain a statistically significant sample of these bigger drops. On the other hand, because there are many more smaller drops, too large a sample area will lead to unacceptable errors as two drops are sampled simultaneously.

The J–W disdrometer incorporates a rigidly sprung toadstool-shaped receiver, which has a striking area of 50 cm^2. Earlier impaction devices had an unacceptably long "dead time" following one drop before the instrument was ready to receive another (Mason, 1971), but in the J–W disdrometer an automatic compensation force reduces the ringing following impact so that the dead time can be as short as 1 ms. As a result of electronic processing, the output is proportional to neither the momentum nor the force, but varies as D^n, where D is the diameter, and n is in the range 4.3 to 3.1 (Joss and Waldvogel, 1977). Concentrations may then be calculated using the terminal velocities of Gunn

and Kinzer (1949). Rowland (1976) and Kinnell (1976) have considered the effect of up- and downdrafts on the terminal velocity. Although Kinnell's conditions were too severe (drop fall speeds deviated by up to 50%), Joss and Waldvogel (1977) computed that for "fairly strong" horizontal winds of 6 m s^{-1} at 2 m above ground, the turbulence would introduce a standard deviation of 10% in the velocity which corresponds to a 4% change in diameter. Donnadieu (1980) and Stow and Jones (1981) present some evidence for changes of velocity of this order in fairly placid conditions. For winds of 20 m s^{-1} the turbulence will be much greater and the errors more serious. At these speeds the raindrops are traveling nearly horizontally, but providing the fall angle of the drops is greater than that of the "toadstool" the sample area is unaffected. For winds of 20 m s^{-1} the acoustic interference of the wind, and the spurious signals produced by the variable drag of the gusty wind on the device itself will both lead to a loss of sensitivity to small drops.

The Knollenberg Optical Array Spectrometer uses a linear array of photodetectors as a size-measuring grid in a typical shadowgraph-type imaging system. A single array is sufficient for airborne measurements; in the 1970 paper (Fig. 24) two arrays spaced apart are proposed for ground-based measurements of raindrop size and fall velocity. The array elements are typically 100 μm in diameter and the array separation is slightly larger than the expected maximum drop size. The greatest number of photodetectors occulted by a passing drop automatically yields the drop diameter, and its fall velocity is inferred from the transit time. In common with all instruments which rely on sizing drops and deriving their velocity as they pass through two successive sampling areas, this device seriously undercounts in windy conditions. As the wind increases, the drops do not fall horizontally and an increasing number of drops detected at the upper sampling area fail to pass through the lower one. This problem has been considered by Griffiths (1975) and Rinehart (1983). One approach (Bradley and Stow, 1974) is to tilt the instrument so that the sampling areas are normal to "the mean rain direction", but this is not really satisfactory because this direction is not well defined if various drop sizes are present. Rinehart (1983) shows that for Jones' (1959) drop camera a 20 m s^{-1} wind would lead to detection efficiencies of less than 5% for millimeter drops and only 10% for larger ones. This camera had an aspect ratio of two (vertical separation twice the horizontal); for the Knollenberg (1970) design, the aspect ratio is nearer to unity and the efficiencies would be closer to 10% and 20%, respectively. Stow and Jones (1981) suggest that these low drop-detection efficiencies can be allowed for by applying a large correction factor dependent upon an instant measurement of the wind; however, this undercounting will lead to a proportionately longer time to achieve a statistically significant sample, and the wind itself might change considerably during this long time. In a more recent paper Hosking et al. (1985) calculate the correction factors for the Jones' (1959) camera for speeds of up to 40 m s^{-1} and for their own device (Stow and Jones, 1981). This latter device has an even larger aspect ratio and so the correction factors are over an order of magnitude, although, rather surprisingly, for their instrument they only extend the analysis to 1 m s^{-1} speeds.

A better approach is to detect the maximum number of diodes in shadow using only a single array, as in the Knollenberg GBBP-10 ground-based precipitation probe, the vertical velocity and hence the concentration being derived from the maximum occultation time of the diodes. Problems will arise with the sampling area if the raindrops do not fall vertically. For example, millimeter drops will fall at an angle $\tan^{-1}5$ to the vertical in a wind of 20 m s^{-1}. Using 64 diodes separated by 200 μm, this means that 80% of the millimeter drops will shadow one of the end diodes; for 2 mm drops the figure is nearly 100%. The velocity will be underestimated and the pulses usually rejected because they shadow an end diode. One way to overcome this would be to record the time evolution of the illumination of each diode, (as for the 2D probe), and from this information to reconstruct the trajectory of each particle. As the wind changes the trajectories alter, but it would be possible to keep track of the changing sample area, and calculate the velocity and size of each particle and so derive the concentration. As we show in the next section, there is a simpler method of deriving concentration from the output of a single photodiode without needing to calculate trajectories and velocities and correct for varying sample volumes.

3. Operating principle of the new disdrometer

The need to obtain reliable measurements of raindrop sizes and concentrations in windy conditions has prompted the development of the Paired-Pulse Optical Disdrometer (P-POD). In contrast to the flux-measuring instruments described previously, this device is able to measure raindrop concentrations without any knowledge of the various drop velocities. In essence, it senses the size of a raindrop as it enters and exits from a sample volume, V; by timing such events the transit time, t, of the drop through the sample volume may be found. During a total sample time, T, many drops will pass through the sample volume, but if we restrict our attention to drops within a given size range, we can sum the various transit times of the drops (Σt), and can say that for a fraction of the total sample time, $\Sigma t/T$, there was a drop within this size range in the volume V. In other words, the number of drops in volume V is $\Sigma t/T$. The next step is to calculate the number of drops in unit volume, which is the concentration, N, and is given by

$$N = \sum t/(VT). \quad (1)$$

This relationship is independent of the drop velocity. Suppose that owing to wind or turbulence the velocity of the drops increases by a factor of two but that their volume concentration is unchanged. In this case, the flux of the particles crossing the sample volume V doubles, and any method which derives the concentration from the flux would detect a spurious increase in drop concentration. However, the factor $\sum t/T$ will be unchanged because, although twice as many drops are detected, each drop will on average cross the sample volume in half the previous time.

In our implementation of this scheme a cylindrical sample volume, V, is defined optically as shown in Fig. 1. A high-intensity light source, S, and collimating lens, C, illuminate the sample volume with parallel light. In front of the focusing lens, F, is placed a mask, M, which permits only a thin annulus of light (thickness d and radius a) to pass through and be collected at the photodiode, P. This annular mask defines the radius, a, of the cylindrical sample volume, and permits only a thin sheath of light (thickness, d) to be gathered by the detector. If d is much smaller than any drop diameter, then the reduction in light level as the drop enters or leaves the sample volume will be proportional to the drop diameter. As a drop passes in and out of the sample volume, two pulses of equal amplitude will be detected as displayed in curve a of Fig. 2. For a given drop velocity the separation time, t, of the two pulses will vary with the position of drop incidence on the annulus, Fig. 2a being the longest time. The shortest separation time which can be resolved will occur for the drop trajectory shown in Fig. 2b, where, when the drop has penetrated the maximum distance into the sample volume, the perimeter of the drop is still just touching the annulus. In Fig. 2c, grazing incidence causes a single pulse. In order to derive drop concentrations, it is necessary to reject single pulses and to recognize equally sized pulse pairs and compute their transit times and amplitudes.

A further advantage of this technique now becomes apparent. In many devices, the sample volume is limited in size because of the apparently fundamental restriction that only one drop at a time be in the sample volume (see Figs. 1 and 3 of Stow and Jones, 1981). This restriction may be relaxed for this instrument. Several drops may occupy the sample volume at the same time. Figure 2d shows a typical waveform, and the ambiguity is absent provided that the drops are not of the same size and that they do not produce overlapping pulses by entering or leaving the sample volume simultaneously. The choice of a cylindrical shape for the sample volume ensures that when the wind blows and the drops are not falling vertically, the projected sample area is the same and a reasonable number of drops is still sampled.

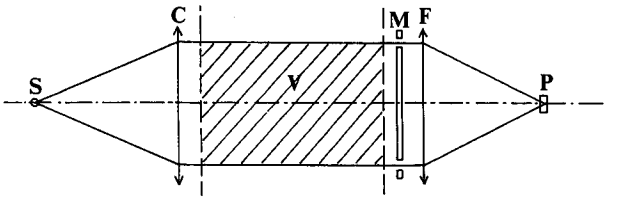

FIG. 1. Schematic representation of the sampling volume V (shown hatched); S: light source; C: collimating lens; M: annular mask; F: focusing lens; P: photodiode detector.

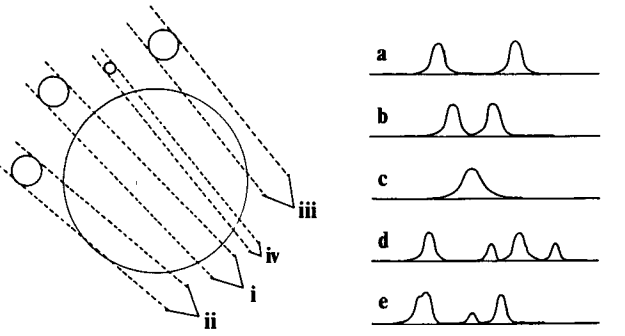

FIG. 2. The variation of light level produced by various drop passages across the annulus. (a) pulse pair produced by trajectory i; (b) pulse pair at the limit of resolution—trajectory ii; (c) single pulse produced by grazing incidence iii; (d) double pulse pair produced by drops i and iv present in the volume together; (e) ambiguous overlapping pulse pairs if drops i and iv enter the sample volume simultaneously.

Our analysis has assumed perfectly collimated light and geometric shadows unaffected by diffraction. Consideration should also be given to any "shadowing" caused by strong winds blowing along the axis of the instrument. In the following section, we discuss the optimum dimensions needed to attain this goal, while maintaining a sufficient sample volume so that a statistically significant sample may be obtained in a reasonable time.

4. The new disdrometer

Figure 3 is a scaled side elevation of the P-POD. On the left is the tube (C) containing the source and collimating optics. The right-hand portion consists of a tube (F) containing the mask, focusing optics and photodiode, and an adjoining sealed housing (E) for the front-end amplifiers and line-driving circuits. The tubes containing the collimating and focusing optics are coaxially mounted and are positioned well above the base of the instrument to prevent splash particles passing through the sample volume. The power supply unit is housed within a sealed box (I) and additional weatherproofing is provided by means of a guard (G) which fits over the collimating tube.

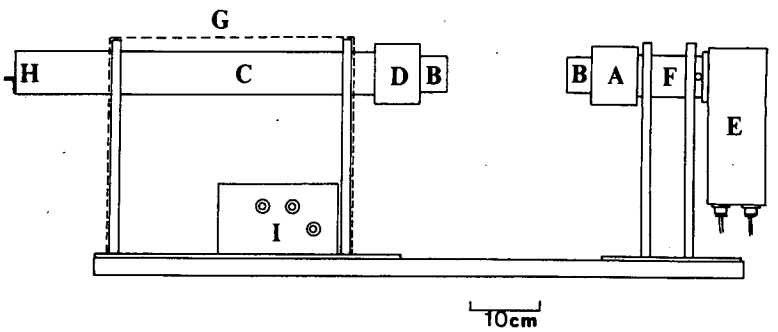

FIG. 3. A section through the new P-POD disdrometer. The light is collimated in the left-hand side and detected on the right-hand side. A and D—collars holding lenses and heaters, B—baffles (see Fig. 4), C—collimating optics, D—focusing optics, E—receive electronics, G—guard, H—halogen light source, I—power supplies.

The sample volume is 170 mm long and 30 mm in diameter giving a volume of 120 cm^3 and an area presented to the rain of 50 cm^2. It is shown in section 5 that this volume is large enough to enable good sampling of the larger drops, but not so large that overlapping pulses occur when two drops enter or leave the sample volume simultaneously. The beam divergence and diffraction effectively limit the maximum length to 170 mm if drops down to 300 μm are to be detected (see section 6). Uniform illumination of the 30 mm diameter annulus can be simply achieved using a single lens. The length of the sample volume may be varied (between 50 and 200 mm) by moving the collimating tube backward or forward along its supports. This flexibility allows the operator to concentrate on the more numerous smaller drops (smaller sample volume) or on the larger drops.

The sample volume is illuminated by a high-intensity 6 V, 20 W halogen source retained in a movable holder (H) at the far end of the collimating tube. The filament is rectangular in shape and has a small area of less than 3 mm^2. The bulb holder permits movement of the source in the vertical. Collimation of the white light is achieved by means of a 500 mm focal length lens positioned within the collar D. The 100 mm focusing lens is situated inside the collar A, along with the mask, and the photodiode is positioned at the rear of F, in the focal plane of this lens. The mask is wholly coated with a thin opaque film except for a very precise annular region 30 mm in diameter and 100 μm wide. The width of this light-transmitting annulus is specified to ± 1 μm and the transmission around the annulus is uniform to better than one part in 100. Such precision is easily achieved using current mask technology. The photodiode itself has a 124° acceptance cone and a surface area of 7.5 mm^2. This arrangement of diode, lens and mask ensures that negligible extraneous light is detected and that the device can operate in sunlight; the acceptance angle at the mask is less than 0.02 radians, and so does not extend outside the outer edge of the baffles (B in Fig. 3) at the end of the collimating tube. The diode is mounted so that it can be moved horizontally within the focal plane of the 100 mm lens.

Two data cables transmit analogue signals from the front-end electronics package (E) to a remote microcomputer. The first stage of the package comprises a current to voltage converter, and the dc output of this amplifier is sent to the computer so that the overall illumination level may be monitored. The second stage consists of an ac amplifier, and changes in the light level caused by the raindrops are sent along the second data cable. The frequency response required of these amplifiers is discussed in section 5a.

The collars A and D contain, in addition to the system lenses, arrays of resistive heaters each rated at 9 W. Each heating system consists of individual elements which butt internally against a clear glass plate placed external to the lens and mask. These prevent the formation of condensate on the optical surfaces. Cloud droplets and raindrops also run the risk of interfering with the transmission properties of the optics by being blown or otherwise driven onto these surfaces, so an additional intricate baffle system is installed within each of the sections B of the instrument tubes. The baffles (Fig. 4) are not dissimilar to the porcelain insulators seen on high-tension electricity cables. Each baffle consists of a cylindrical stalk and concentric, regularly spaced discs 28 mm in diameter. The whole one-piece unit is affixed to the protective glass plate such that the discs are offset with a series of ribs on the internal surface of the outer tube. The ribs and discs provide a convoluted air gap within the tube about 50 mm long, 30 mm in diameter and 4 mm in width, which restricts the movement of any drops within the casing but allows the passage of light through the baffles from the collimating optics to the mask. The entire baffle system is easily removed, enabling the glass plates to be cleaned at regular intervals.

The instrument is designed so that it is insensitive to wind vibration and flexing when operating in the

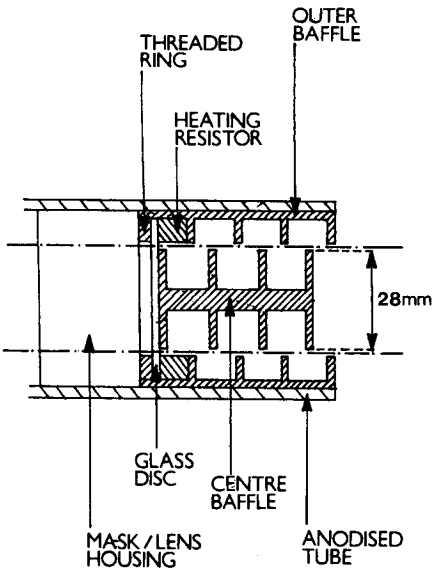

FIG. 4. An expanded view of the baffles ("B" in Fig. 3) showing the arrangement to minimize drop impaction on the optics.

field, and also so that setting up and alignment of the optics is not critical. The image of the source formed on the sensitive area of the photodiode is less than 1 mm in diameter. The image is positioned in the center of this sensitive area by moving the source holder (H) in the vertical and the diode itself in the horizontal direction while monitoring the dc illumination level. When the image is centrally placed, relative movements of the receive and transmit optics of up to 2 mm may be tolerated. The 4 mm baffle gap will also accommodate this movement.

In the remote signal processing circuitry, the dc illumination level is periodically sampled. As the optics become progressively dirty, this dc level falls slightly, giving a good indication of when the glass plates supporting the baffles need to be cleaned. This layer of dirt tends to be uniformly spread on the glass, thus leading to a slight reduction in all the pulses from the drops, and so the dc level may be used to correct for this in the software. For the ac shadow pulse signals, the external processing circuitry first provides an attenuator for use with the calibration drops (see section 7) followed by a low-pass (50 Hz) filter to remove low-frequency noise caused by scattering off aerosol and cloud particles moving through the sample volume. A unique peak detector, with no overshoot and no dependence on pulse rise time then senses the maximum value of the pulse amplitude, converts it to digital form, and generates an interrupt for the Z80 based microcomputer (NASCOM—manufactured by Lucas Logic). The computer then reads this digital voltage and the time; the accuracy of this timing is specified in section 5c. The software recognizes equally sized pulse pairs and sorts them into 15 channels depending upon the pulse amplitude. When a drop is detected, the appropriate register is increased by the transit time for the drop, and a drop counter is incremented. The concentration is derived from the sum of the transit times, and the drop count is used to compute the error using Poisson statistics.

5. Pulse statistics and signal processing

The signal processing for the disdrometer must be able to detect the peak value of each pulse as a drop enters and leaves the sample volume, to recognize equally sized pulse pairs and to measure the elapsed time between the pulses. In this section, we present an analysis of the expected distribution of shapes of individual pulses and the separation times expected, so that an accurate measuring system can be designed. We shall also consider the statistics of multiple occupation of the sample volume and the algorithm which can recognize and correct for this potential ambiguity.

a. Individual pulse rise times

Table 1 gives the widths of the individual pulses for the two extreme examples of drops falling at terminal velocity (Gunn and Kinzer, 1949), and of drops moving with a velocity of 20 m s^{-1}. The possible pulses which may be encountered are best discussed with reference to Fig. 2. The shortest individual pulses will occur when the drop trajectory is normal to the annulus, as in curve a in the figure. The longest individual pulse will be found for the more grazing type of collision where the two pulses are just resolved (curve b in Fig. 2); for this case, the minimum transit distance is also tabulated. As the drops approaching the sample volume are randomly positioned in space, a simple integration shows that the average pulse width will be 1.57 times these minimum values. The range of conditions results in pulse widths varying from 15 μs to 2.2 ms, or to pulse rise times of half these values. This response may be easily achieved using a photodiode detector in the photovoltaic mode (for minimum noise) which feeds current into the virtual ground of a conventional operational amplifier configured as a current to voltage converter.

b. Pulse separation times

The range of minimum and maximum pulse separation times are also shown in Table 1. The shortest time of only 210 μs occurs at 20 m s^{-1} for the small drop with the minimum length trajectory, and the longest separation time of 26 ms is for a small drop falling at terminal velocity with the maximum trajectory. Because the trajectories are randomly positioned in space, the average pulse separation time will be at least 78% of the maximum tabulated value (i.e., 1.17

TABLE 1. Values of the widths of individual pulses and pulse separation times (PSTs) of pulse-pairs expected for drops of various sizes moving at a) terminal velocity and b) 20 m s^{-1}.

	(a) Drops falling at terminal velocity						(b) Moving at 20 m s^{-1}		
Diameter	Velocity (m s^{-1})	Min pulse width (μs)	Max pulse width (ms)	Min transit distance (mm)	Min PST (ms)	Max PST (ms)	Min pulse width (μs)	Min PST (μs)	Max PST (ms)
300 μm	1.15	260	3.95	4.2	3.6	26	15	210	1.5
500 μm	2.04	245	2.93	5.5	2.7	15	25	277	1.5
1 mm	4.03	248	1.92	7.5	1.9	7.5	50	375	1.5
2 mm	6.49	308	1.99	11	1.7	4.6	100	550	1.5
4 mm	8.83	453	2.20	15	1.7	3.4	200	750	1.5

ms for the 20 m s^{-1} case). In principle, the accurate electronic measurement of such a range of separation times presents no problem. Transit times are presented to the computer as 16 bit numbers, measured in units of 8 μs, so the maximum value of t which can be held for one particular drop is 0.5 sec, far in excess of the expected maximum transit time of 26 ms for a 300 μm drop. A 16 bit overflow counter is incremented every time Σt exceeds a multiple of 0.5 sec, so in theory a maximum accumulated transit time for drops of a particular size exceeds 8 h. This allows for sample periods of variable lengths; longer periods obviously lead to better statistics. For example, a count of 200 drops results in a sampling error, according to Poisson statistics, of 7% in the estimated concentration. Doubling this drop count reduces the error to 5%. Joss and Waldvogel (1969) have considered the time required to obtain a significant sample; for the P-POD their curves for a sample area of 50 cm^2 are appropriate. As indicated earlier, P-POD software keeps track of drop counts and computes errors in estimated concentrations.

c. *Multiple occupation of the sample volume*

If the concentration of raindrops is N and the sample volume is V, then the average probability of finding one drop within the volume is $\lambda = NV$. Poisson statistics then give the probability of finding m drops in the volume as

$$P(m) = e^{-\lambda}\lambda^m/(m!). \quad (2)$$

Table 2 summarizes the results for light, heavy and extremely heavy rainfall assuming a Marshall–Palmer (1949) drop size distribution. Figure 2d shows the amplifier output expected when two dissimilar-sized drops are present in the sample volume at the same time. The fraction of these events as compared to the normal pulse pair shown in Fig. 2a is given by $P(2)/P(1)$ $(=\lambda/2)$ in Table 2. The fraction of triplet events $(P(3)/P(1) = \lambda^2/6)$ is also tabulated. It is relatively straightforward for the software to recognize the overlapping pulse pairs and compute the correct transit time of the two drops; our implementation allows up to six dissimilar-sized drops to be present. When the drops are the same size the ambiguity remains, and the software will interpret the data as two successive matching pulse pairs, effectively adding, on average, values of t of half the true magnitude to the accumulating total transit times. The proportion of pulse pairs affected with this problem is shown in Table 2 for the size ranges 300–600 μm and 1.2–1.5 mm. It can be seen that this technique effectively disposes of the multiple occupation restriction. For the 100 mm h^{-1} rainfall rate, instead of losing 18% of all drops, for drops in the 1.2–1.5 mm range the underestimate is just 1.6% and will be even lower for larger drops.

d. *Dead times*

The correction scheme outlined above will fail if two drops enter or leave the sample simultaneously and result in overlapping pulses as shown in Fig. 2e. To

TABLE 2. The concentrations of drops of various size ranges assuming a Marshall–Palmer size distribution, and the ratios of the probabilities of multiple occupation of the sample volume of 120 cm^3.

	All drops > 300 μm			300–600 μm		1.2–1.5 mm	
Rain rate (mm h^{-1})	N (m^{-3})	$P(2)/P(1)$ (%)	$P(3)/P(1)$ (%)	N (m^{-3})	$P(2)/P(1)$ (%)	N (m^{-3})	$P(2)/P(1)$ (%)
1	570	3.1	<0.1	390	2.3	10	0.05
10	1,482	8.9	0.5	761	4.5	79	0.5
100	3,009	18	2	1,117	7.0	269	1.6

calculate the probability of this occurrence, we note that if a drop of diameter D has its center within a distance of $D/2$ of the annulus it will give rise to a pulse, that is to say if the drop center is within the volume $2\pi aDl$, where a is the radius of the annulus and l its length. If we now consider a Marshall–Palmer distribution of raindrops

$$N(D) = N_0 \exp(-\Lambda D) \tag{3}$$

where N_0 is constant and $\Lambda = 4.1R^{-0.21}$ for a rainfall rate of R mm h^{-1}, we may integrate over all drop sizes to find that the probability of one drop giving a pulse is

$$\lambda = 2\pi alN_0/(\Lambda^2). \tag{4}$$

For rain rates of 1, 10 and 100 mm h^{-1} then λ is 0.7%, 2% and 4%, respectively. The probability of overlapping pulses is $\lambda/2$.

The response time of the electronic processing should also be considered. On sensing a pulse, the peak detector circuit generates an interrupt. The response time to this interrupt, and the execution of the procedure which reads and so clears the peak detector for the next pulse, is less than 50 μs. The processing of the pulse information takes longer, but will constitute a problem when consecutive drops arrive within 50 μs of each other. For drops at terminal velocity, we see from Table 1 that this dead time of 50 μs is a negligible fraction of the individual pulse width and so the overlapping probability is still $\lambda/2$. The dead time only becomes significant for the smallest drops and for a 20 m s^{-1} windspeed, which is equivalent to a doubling of the pulse width. The overlapping probability is still small, but is increased from $\lambda/2$ to λ.

It is interesting to compare these very low values of dead time with those of other instruments. The instrument of Stowe and Jones (1981) has a dead time of 50 ms and their Fig. 10 shows that in 10 mm h^{-1} rainfall they will fail to detect 40% of the drops. The J–W disdrometer has a dead time generally of only 1 ms, but if the first drop (diameter D_1) is more than three times the size of the following drop (D_2) the response time, t_r is

$$t_r = 60 \ln(D_1/D_2). \tag{5}$$

For 10 mm h^{-1} rainfall this leads to a loss of only 5% of 300–600 μm sized drops, and for 100 mm h^{-1} 37% of drops in this range and 8% of drops 600–900 μm will escape detection. This does affect spectral shape, but, as the authors comment, this undercounting will not affect values of R and Z (radar reflectivity) derived from the instrument.

6. Diffraction and beam divergence

Diffraction constitutes a fundamental limit to the accuracy of the shadowgraph technique. Knollenberg (1970, Fig. 7) plots isodensitometer traces across shadows produced by spherical particles in white light as a function of distance from the particle. The distances are expressed in terms of z, defined as r^2/λ, where r is the particle radius and λ the wavelength of light. A perfect geometric shadow is produced when $z = 0$ but as z increases the shadows become broader and less deep. The signal detected by the annulus in the P-POD device is the integrated light along a slice through the shadow and is proportional to the area under the isodensitometer traces. For $z = 1$, 2 and 3, this signal is estimated to be 89%, 73% and 65%, respectively, of the level for the perfect shadow at $z = 0$. The diffraction effect increases rapidly as particle size diminishes. For a 600 μm drop $z = 1$ corresponds to about 180 mm, but only 45 mm for the 300 μm drop. The average loss of signal for an ensemble of 600 μm particles placed randomly within the sample volume, which is from 50 to 220 mm from the annulus, will be less than 7%, but for the 450 μm particle this loss will be 15%.

With the present configuration of P-POD, beam divergence is a more serious limit than diffraction. The finite size of the light source results in the collimated beam, having a spread of 3 mrad. A series of numerical integrations has been carried out to estimate the magnitude of the problem. When the angle subtended (α) by the drop at the annulus is equal to the beam divergence, as depicted in Fig. 5, the central totally dark region disappears and only penumbra remains. If we call this angle α_c, the critical angle, then integrations can be carried out for various multiples of α_c, and the results can be applied to different sized drops at various distances from the annulus. Figure 6 shows computed profiles across the shadows for various multiples of α_c. The technique adopted was to solve the inverse problem of the light cast by a circular aperture; the light source was split up into a series of rings and the resulting radial intensity distribution computed, then the contributions of the rings were summed.

Two numerical checks were carried out: the illumination computed on the axis ($D = 0$) should agree with the analytical value, and the total light energy integrated over the whole area of the shadow should

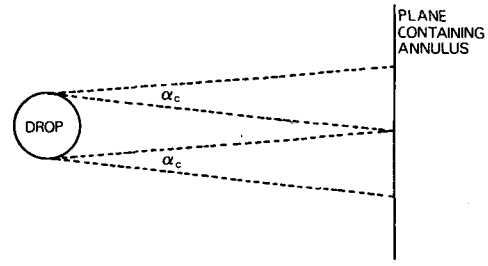

FIG. 5. The effect of beam divergence on the shadow. The angle subtended by the drop at the annulus is equal to the beam divergence, and the central shadow region of total shadow just disappears leaving only penumbra. This angle is defined as α_c.

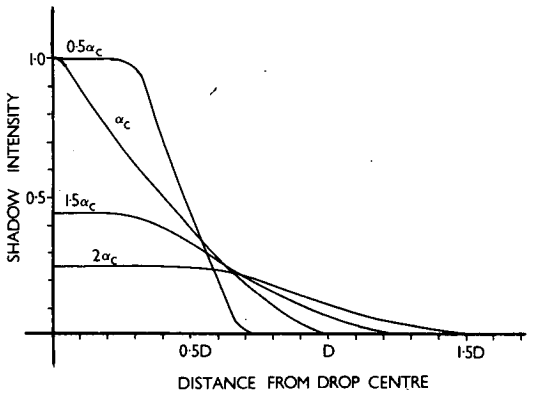

FIG. 6. The radial variation of light intensity across the shadow cast for various multiples of α_c. D is the drop diameter.

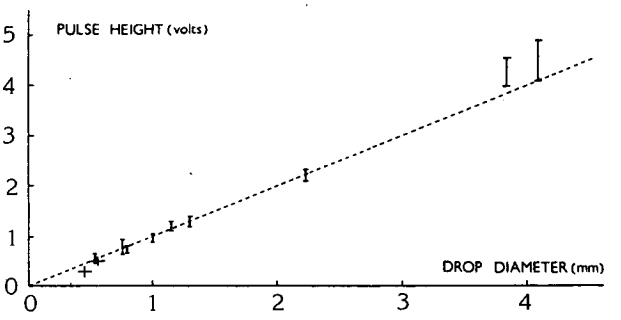

FIG. 7. Calibration curve for the disdrometer using drops produced in the laboratory.

be the same as that for perfect collimation—the beam divergence merely redistributing this energy in space. As before, the signal detected by the annulus is equal to the area under the curves in Fig. 6. Some sample values are displayed in Table 3, together with the fractional reduction in signal expected for 300, 600 and 900 μm drops at the minimum and maximum distances from the annulus (50 and 220 mm). According to these figures, if a linear response with pulse amplitude is assumed, then pulse pairs apparently corresponding to drops in the ranges 300–600 and 600–900 μm will, in fact, on average result from drops in size ranges 400–660 and 660–945 μm, respectively.

7. Calibration and correction factors

The disdrometer was calibrated in the laboratory and the results are displayed in Fig. 7. Drops ranging in diameter from 540 μm to 2.25 mm were produced by an oscillating diaphragm set in a pressurized flow of water which then discharged through a hypodermic needle (Atkinson and Miller, 1965). Smaller drops down to 400 μm were formed by raising the water in a fine capillary to a high potential (after Vonnegut and Neubauer, 1952). A fine spray of charged droplets was produced in this manner, and they were individually sized by collecting them in oil and viewing through a microscope. Drops larger than 2.5 mm were produced by allowing water to flow naturally through various sizes of hypodermic needles. These larger drops oscillated with far greater amplitudes than natural raindrops; for example, 4 mm drops released from a height of 2 m produced individual pulses varying by as much as 10% of the mean value as shown by the vertical bars in Fig. 7. The horizontal bars for the small drops show the uncertainties in the drop sizes inferred from microscope readings. The pulses from drops smaller than one millimeter varied with drop position in the beam; the higher amplitudes shown in the Fig. 7 are from drops closest to the mask and the lower amplitudes are for the maximum distance (220 mm) from the mask.

The 2.2 mm drops were used for calibration purposes because the signals they produced agreed with theoretical values derived from considering the fraction of the total light incident upon the annulus which was obscured by a drop of this size. The total incident light is measured by the dc signal level. For these 2.2 mm drops, the attenuator was set so that 2.2 V pulses were produced. Departures from linearity are apparent in Fig. 7 for drops below 1 mm and for those above 3 mm. The loss in signal for drops below 1 mm size, and the dependence of signal with position within the sample volume, may be explained in terms of beam divergence. The values in Table 3 and accompanying computations suggested that if a linear response was assumed, then drops which gave signals equivalent to 900, 600 and 300 μm particles would on average be only 945, 660 and 400 μm, respectively. Examination of Fig. 7 shows that the deviation from linearity does correspond to these values, and so the concentrations recorded by the disdrometer in the lower two channels were corrected in accordance with these computations.

Drops above 3 mm are significantly affected by their oblateness. The drop diameter, as measured by the disdrometer was on average 10% greater than the calculated diameter for a 4 mm drop. These deviations, shown in Fig. 7, are in agreement with the drop shape computations of Pruppacher and Pitter (1971). Their

TABLE 3. The pulse amplitudes expected for various sized drops in a beam divergence of 3 mrad at a distance of 50 mm and 220 mm from the mask and the mean pulse over this range. Unit signal for zero divergence.

Size (μm)	Distance from mask (mm)		
	50	220	Mean
300	0.95	0.37	0.65
400	0.96	0.51	0.75
600	0.99	0.76	0.90
900	0.99	0.91	0.95

model showed that when a raindrop of volume equivalent to a 4 mm diameter sphere falls at terminal velocity, the horizontal diameter is about 12% greater than 4 mm and 3% for a 3 mm drop. However, these correction factors are strictly dependent upon the wind speed; if the drops are traveling horizontally, P-POD will underestimate their size. In theory, a wind-dependent correction factor could be derived by calculating the main transit times for one particular drop size, which gives a mean resultant velocity and hence the angle of fall of the drops. In practice, this has not proved necessary. Such large drops are so infrequent that this second-order correction is less than the Poisson sampling error. An attempt to apply wind-dependent correction factors might be justified at rainfall rates of 100 mm h^{-1}, but at 10 mm h^{-1} for rain with a Marshall–Palmer distribution, the concentration of 4 mm drops is only 1% of the 2 mm drop concentration.

Two other effects should be considered. First, corrections for signal loss from optical transmission losses can be applied if the instrument is left unattended for many days, but in practice it is more convenient to clean the glass when the light level detected by the dc monitor level falls appreciably. Second, the effective sampling volume decreases for the larger drops because there is less space through which they may pass and give rise to two resolvable pulses. If the length of the sampling volume is l, the radius of the annulus is a, then for a particle of diameter D the effective sampling volume V_E is given by

$$V_E = \pi(a - D/2)^2 l. \tag{6}$$

This effective volume should be used in Eq. (1) to calculate the drop concentration. This correction can be significant; for a 3 mm drop V_E is 81% of V.

The instrument is normally set up so that 2.2 mm drops produce 2.2 V pulses and pulse pairs are sorted into 15 channels each 320 mV wide. Accordingly, for a linear response, channels 1, 2 and 3 would correspond to mean sizes of 480, 800 and 1120 μm (or size ranges 320–640, 640–960 and 960–1280 μm). Because of the signal losses due to beam divergence discussed previously, the mean size for the first three channels was corrected to be 570, 860 and 1140 μm.

Finally we note that, in common with all optical instruments, the optical axis should be maintained perpendicular to the wind. If the wind veers by 45° with no realignment, then shadowing will reduce the sample volume by up to 10%.

8. Preliminary results and conclusions

The novelty of the P-POD lies in its ability to derive drop concentrations without prior knowledge of their fall velocities. Consequently, this makes the disdrometer particularly suited to operation in inclement weather conditions where surface air motions are not inconsiderable. Equation (1) may be rewritten as

$$N_T = \frac{1}{T}\sum_d \left(\frac{t_d}{V_d}\right) \tag{7}$$

where t_d are the drops' times of flight summed over each channel, V_d are the channels' effective volumes from Eq. (6), and T is the sampling period. Then N_T may be described as the "time-of-flight" drop number concentration.

This method of the calculation of N may be compared with that of the "flux" number concentration, N_F which is derived from the flux of raindrops across an equivalent sampling area. This procedure involves the drops' velocity spectrum explicitly as is expressed by the equation

$$N_F = \frac{1}{T}\sum_d \left(\frac{n_d}{A_d v_d}\right) \tag{8}$$

where n_d are the drop counts per channel, v_d are the channel-averaged drop fallspeeds, and A_d are the channels' effective sampling area.

In situations where the surface windspeed is significant, raindrops will pass through the sample volume with velocities in excess of their still-air speeds. The increase in velocity will be felt more by the smaller drops, which would in calm conditions be falling at only 2 or 3 m sec^{-1}. Under such conditions, using the Gunn and Kinzer (1949) drop velocity spectrum in Eq. (8) would give apparently greater number concentrations N_F for the smaller drops. Figures 8 and 9 are plots of the disdrometer-derived averaged drop size

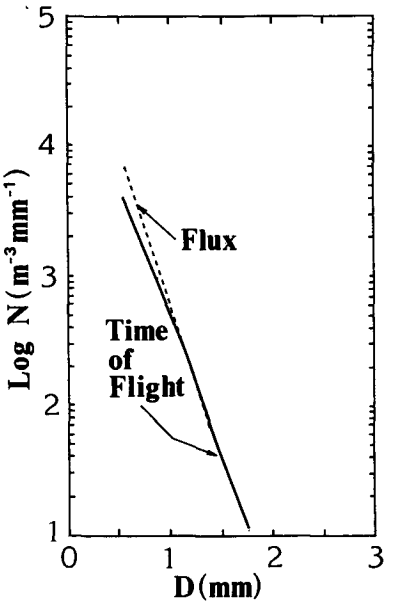

FIG. 8. A comparison of spectra observed by the P-POD using the time of flight (solid line) and the flux (dotted line) methods in a wind speed of 5 m s^{-1}. The flux method overestimates the concentration of the smaller drops.

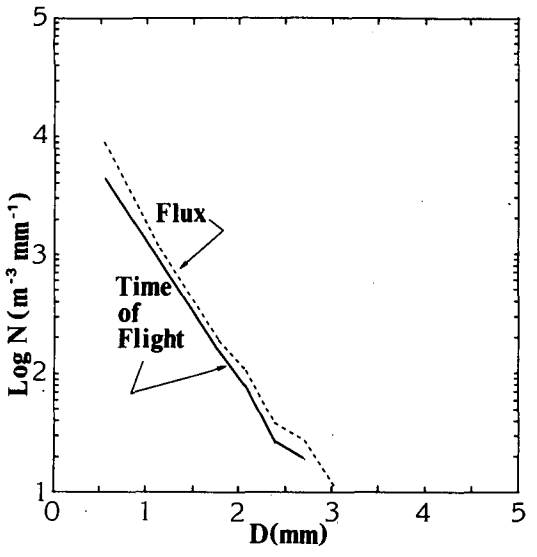

FIG. 9. As for Fig. 8, but in a stronger wind of 13 m s^{-1} the flux method overestimates the concentration of drops of all sizes.

distributions for two situations which show quite different surface wind conditions. Figure 8 applies to a 1-h period of light rainfall which occurred in a gentle breeze of about 5 m s^{-1}. Large drops are little affected by the surface wind and their fallspeeds remain virtually unchanged. For the smaller drops, however, which have still-air speeds of less than 3 m s^{-1}, the surface wind considerably affects their trajectories and velocities. This is reflected in Fig. 8; the "flux" method of calculation overestimates the concentrations of drops smaller than 1 mm in diameter, and for 500 μm drops the overestimation is by a factor of two. The "flux" and "time-of-flight" concentrations for larger drops are in agreement because these drops are not so readily influenced by the light wind. Figure 9 displays a 60-min averaged drop size distribution obtained in a strong wind ($\sim$13 m s^{-1}). Now even the 2 mm drops are affected by the windspeed and this is seen in the disagreement of the two calculated spectra up to quite large drop sizes. These figures are evidence for the superior time-of-flight technique of obtaining drop size spectra employed by the P-POD, and emphasize the inappropriateness of the conventional flux technique in generally windy conditions.

Cross-calibration tests were conducted between a P-POD and a tipping bucket raingage in light wind conditions and varying rainfall intensities to obtain some idea of the efficiency of the disdrometer in measuring rainfall rates. Figure 10 compares a 2-h period of rainfall which occurred on 14 May 1985, as measured by the tipping bucket raingage with the equivalent accumulated rainfall sensed by the disdrometer. It should be noted that the disdrometer and raingage were positioned within 4 m of each other, although the disdrometer was mounted on a tripod 2 m above the ground. The agreement between the two devices is better than 90%. The mean rainfall rate for the two hours from 1810 UTC is 3.6 mm h^{-1} but in the half hour from 1940 UTC the mean intensity exceeded 7 mm h^{-1}. Table 4 divides the rainfall period into five sections and compares the gage and disdrometer totals for each section. Although there is a good deal of variation in the agreement between tthe devices for the five sections, it must be appreciated that the gage does show hysteresis between accumulating rainwater and registering a tip, the length of the delay being dependent on the rainfall rate. Consequently, the gage totals can be in error by $\pm$0.1 mm. The period 1819–31 has been omitted from the five sections because there was only one tip of the bucket during this time; it is included in the final row labeled "total."

For these short time intervals, the disdrometer sampling time is also significant. From the analysis of Joss and Waldvogel (1969) for a 50 cm^2 sample area, a sample time of 200 sec is required to estimate a 1 mm h^{-1} rain rate to within 8%. To achieve an accuracy of 4% an 800-sec sample is needed. Consequently, the agreement is much better than indicated. The combined sections in Table 4 show that over the entire rainfall period the disdrometer underestimates the gage total by only 7%.

These field results demonstrate the efficient performance of the new device. In light wind conditions, rainfall rates calculated from a number of integrated drop size spectra are found to agree to within a few percent of the bulk measured values obtained by a high-precision tipping bucket raingage. In high winds, raingages cannot be used for adequate comparison, but it is shown that disdrometers which derived drop concentrations from a measurement of drop flux give spuriously high values, and that using the new 'time-of-flight' method the P-POD provides more accurate in-

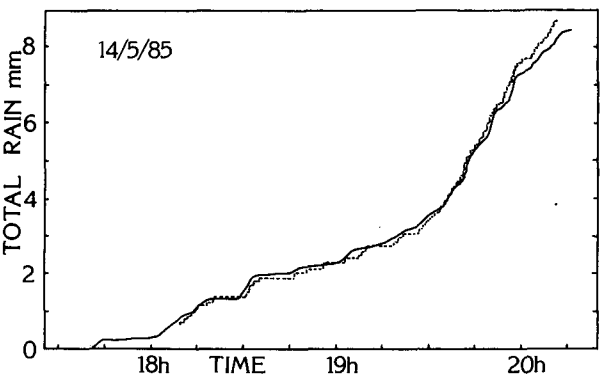

FIG. 10. Total rainfall observed with a tipping bucket raingage (dotted line) and rainfall computed from disdrometer concentrations (solid line) on 14 May 1985. Comparison shows the totals agree to within 7%.

TABLE 4. Comparison of the rainfall rates derived from the tipping bucket raingage and the integration of the disdrometer spectra for the data displayed in Fig. 10 on 14 May 1985.

Section	Time (UTC)	Duration (min)	Gage total (mm)	P-POD total (mm)	Agreement DT/GT	P-POD rate (mm h^{-1})
I	1809–1819	10	0.7	0.55	0.78	3.3
II	1831–1835	4	0.4	0.45	1.12	6.7
III	1835–1927	52	1.3	1.21	0.93	1.4
IV	1927–2000	33	4.5	4.0	0.91	7.2
V	2000–2016	16	1.2	1.17	0.975	4.4
Total	1809–2016	127	8.2	7.62	0.93	3.6

formation. The lower drop-size cutoff for the present instrument is set by the beam divergence from the finite dimensions of the light source. A laser would have smaller beam divergence but would require high-quality lenses and beam expanders and any dirt on exposed surfaces could result in fringes. If the beam divergence could be reduced by a factor of two, the fundamental limit due to diffraction would be reached. At present, such a reduction in light intensity leads to an unacceptable signal-to-noise ratio in the amplifier output. We are currently exploring techniques using lower noise detectors and amplifiers.

Acknowledgments. We would like to thank Peter Kelly for his many useful suggestions and for his help in the workshop. Support for this work was provided by NERC Grant GR3/4785 and ERO grants DAJA-37–80-C-0229 and DAJA-45–83-C-0003. This paper was written while A. J. Illingworth was a Mombushu/British Council visiting scientist with Professor Kikuchi in the Department of Geophysics, Hokkaido University, Japan.

REFERENCES

Atkinson, W. R., and A. H. Miller, 1965: Versatile technique for the production of uniform droplets at a constant rate and ejection velocity. *Rev. Sci. Instrum.*, **36**, 846–847.

Bradley, S. G., and C. D. Stow, 1974: The measurement of charge and size of raindrops: Part 1. The disdrometer. *J. Appl. Meteor.*, **13**, 114–130.

Donnadieu, G., 1980: Comparison of results obtained with the Vidiaz spectropluviometer and the Joss-Waldvogel rainfall disdrometer in a "rain of a thundery type". *J. Appl. Meteor.*, **19**, 593–597.

Griffiths, R. F., 1975: Comments on the measurement of charge and size of raindrops: Parts 1 and 2. *J. Appl. Meteor.*, **14**, 422–425.

Gunn, R., and G. D. Kinzer, 1949: The terminal velocity of fall for water drops in stagnant air. *J. Meteor.*, **6**, 243–248.

Hosking, J. G., C. D. Stow and S. G. Bradley, 1985: Corrections for horizontal winds and wind shear in raindrop size spectrometers. *J. Atmos. Oceanic Technol.*, **2**, 181–189.

Jones, D. M. A., 1959: The shape of raindrops. *J. Meteor.*, **16**, 504–510.

Joss, J., and A. Waldvogel, 1967: Ein Spektrograph fur Niederschlagstropfen mit automatischer Auswertung. A raindrop spectrometer with automatic readout. *Pure Appl. Geophys.*, **68**, 240–246.

——, and ——, 1969: Raindrop size distribution and sampling size errors. *J. Atmos. Sci.*, **26**, 566–569.

——, and ——, 1977: Comments on "Some observations on the Joss-Waldvogel rainfall disdrometer". *J. Appl. Meteor.*, **16**, 112–113.

Kinnell, P. I. A., 1976: Some observations on the Joss-Waldvogel rainfall disdrometer. *J. Appl. Meteor.*, **15**, 499–502.

Knollenberg, R. G., 1970: The optical array: An alternative to scattering or extinction for airborne particle size determination. *J. Appl. Meteor.*, **9**, 86–103.

Lowe, E. J., 1902: Raindrops. *Quart. J. Roy. Meteor. Soc.*, **18**, 242–243.

Marshall, J. S., and McK. W. Palmer, 1948: The distribution of raindrops with size. *J. Meteor.*, **5**, 165–166.

Mason, B. J., 1971: *The Physics of Clouds.* Clarendon Press, 671 pp.

Pruppacher, H. R., and R. L. Pitter, 1971: A semiempirical determination of the shape of cloud and rain drops. *J. Atmos. Sci.*, **28**, 86–94.

Rinehart, R. E., 1983: Out-of-level instruments: errors in hydrometeor spectra and precipitation measurements. *J. Climate Appl. Meteor.*, **22**, 1404–1410.

Rowland, J. R., 1976: Comparison of two different raindrop disdrometers. *Preprints, 17th Radar Meteorology Conference,* Seattle, Amer. Meteor. Soc., 398–404.

Stow, C. D., and K. Jones, 1981: A self-evaluating disdrometer for the measurement of raindrop size and charge at the ground. *J. Appl. Meteor.*, **20**, 1160–1176.

Vonnegut, B., and R. L. Neubauer, 1952: Production of monodisperse liquid particles by electrical atomization. *J. Coll. Sci.*, **7**, 616–622.